

Properties of Cosmic-Ray Sulfur and Determination of the Composition of Primary Cosmic-Ray Carbon, Neon, Magnesium, and Sulfur: Ten-Year Results from the Alpha Magnetic Spectrometer

M. Aguilar,³⁰ L. Ali Cavazonza,¹ B. Alpat,³⁷ G. Ambrosi,³⁷ L. Arruda,²⁸ N. Attig,²⁵ C. Bagwell,¹⁰ F. Barao,²⁸ L. Barrin,¹⁵ A. Bartoloni,⁴¹ S. Başeğmez-du Pree,^{18,*} R. Battiston,^{48,49} N. Belyaev,¹⁰ J. Berdugo,³⁰ B. Bertucci,^{37,38} V. Bindi,²¹ K. Bollweg,²² J. Bolster,¹⁰ M. Borchiellini,¹⁸ B. Borgia,^{41,42} M. J. Boschini,³² M. Bourquin,¹⁶ E. F. Bueno,¹⁸ J. Burger,¹⁰ W. J. Burger,⁴⁸ X. D. Cai,¹⁰ M. Capell,¹⁰ J. Casaus,³⁰ G. Castellini,¹⁴ F. Cervelli,³⁹ Y. H. Chang,⁴⁶ G. M. Chen,^{6,7} G. R. Chen,²⁴ H. Chen,²⁰ H. S. Chen,^{6,7} Y. Chen,^{16,24} L. Cheng,²⁴ H. Y. Chou,⁴⁶ S. Chouridou,¹ V. Choutko,¹⁰ C. H. Chung,¹ C. Clark,^{10,22} G. Coignet,³ C. Consolandi,²¹ A. Contin,^{8,9} C. Corti,²¹ Z. Cui,^{23,24} K. Dadzie,¹⁰ A. Dass,^{48,49} C. Delgado,³⁰ S. Della Torre,³² M. B. Demirköz,² L. Derome,¹⁷ S. Di Falco,³⁹ V. Di Felice,⁴³ C. Díaz,³⁰ F. Dimiccoli,⁴⁸ P. von Doetinchem,²¹ F. Dong,³⁵ F. Donnini,³⁷ M. Duranti,³⁷ A. Egorov,¹⁰ A. Eline,¹⁰ F. Faldi,^{37,38} J. Feng,¹⁹ E. Fiandrini,^{37,38} P. Fisher,¹⁰ V. Formato,⁴³ C. Gámez,³⁰ R. J. García-López,²⁷ C. Gargiulo,¹⁵ H. Gast,¹ M. Gervasi,^{32,33} F. Giovacchini,³⁰ D. M. Gómez-Coral,²¹ J. Gong,³⁵ C. Goy,³ V. Grabski,³¹ D. Grandi,^{32,33} M. Graziani,^{37,38} A. N. Guracho,⁴¹ S. Haino,⁴⁶ K. C. Han,²⁹ R. K. Hashmani,² Z. H. He,¹⁹ B. Heber,²⁶ T. H. Hsieh,¹⁰ J. Y. Hu,^{6,7} B. W. Huang,²⁰ M. Incagli,³⁹ W. Y. Jang,¹³ Yi Jia,¹⁰ H. Jinchi,²⁹ G. Karagöz,² B. Khiali,⁴³ G. N. Kim,¹³ Th. Kim,¹ O. Kounina,¹⁰ A. Kounine,¹⁰ V. Koutsenko,¹⁰ D. Krasnopevtsev,¹⁰ A. Kuhlman,²¹ A. Kulemzin,¹⁰ G. La Vacca,^{32,33} E. Laudi,¹⁵ G. Laurenti,⁸ G. LaVecchia,¹⁰ I. Lazzizzera,^{48,49} H. T. Lee,⁴⁵ S. C. Lee,⁴⁶ H. L. Li,²⁴ J. Q. Li,³⁵ M. Li,^{1,16} M. Li,²³ Q. Li,³⁵ Q. Li,²³ Q. Y. Li,²⁴ S. Li,¹ S. L. Li,^{6,7} J. H. Li,²³ Z. H. Li,^{6,7} J. Liang,²³ M. J. Liang,^{6,7} C. H. Lin,⁴⁶ T. Lippert,²⁵ J. H. Liu,⁵ S. Q. Lu,⁴⁶ Y. S. Lu,⁶ K. Luebelmeyer,¹ J. Z. Luo,³⁵ S. D. Luo,²⁰ Xi Luo,²⁴ F. Machate,¹ C. Mañá,³⁰ J. Marín,³⁰ J. Marquardt,²⁶ T. Martin,^{10,22} G. Martínez,³⁰ N. Masi,⁸ D. Maurin,¹⁷ T. Medvedeva,¹⁰ A. Menchaca-Rocha,³¹ Q. Meng,³⁵ V. V. Mikhailov,³⁴ M. Molero,²⁷ P. Mott,^{10,22} L. Mussolin,^{37,38} J. Negrete,²¹ N. Nikonov,²¹ F. Nozzoli,⁴⁸ J. Ocampo-Peleteiro,³⁰ A. Oliva,⁸ M. Orcinha,²⁸ M. A. Ottupara,²⁴ M. Palermo,²¹ F. Palmonari,^{8,9} M. Paniccia,¹⁶ A. Pashnin,¹⁰ M. Pauluzzi,^{37,38} S. Pensotti,^{32,33} V. Plyaskin,¹⁰ S. Poluianov,³⁶ X. Qin,¹⁰ Z. Y. Qu,²⁴ L. Quadrani,^{8,9} P. G. Rancoita,³² D. Rapin,¹⁶ A. Reina Conde,⁸ E. Robyn,¹⁶ L. Romaneehsen,²⁶ A. Rozhkov,¹⁰ D. Rozza,³² R. Sagdeev,¹¹ S. Schael,¹ A. Schultz von Dratzig,¹ G. Schwering,¹ E. S. Seo,¹² B. S. Shan,⁴ T. Siedenburger,¹ J. W. Song,²³ X. J. Song,²⁴ R. Sonnabend,¹ L. Strigari,^{41,†} T. Su,²⁴ Q. Sun,²³ Z. T. Sun,^{6,7} M. Tacconi,^{32,33} X. W. Tang,⁶ Z. C. Tang,⁶ J. Tian,⁴³ Y. Tian,²⁰ Samuel C. C. Ting,^{10,15} S. M. Ting,¹⁰ N. Tomassetti,^{37,38} J. Torsti,⁵⁰ T. Urban,^{10,22} I. Usoskin,³⁶ V. Vagelli,^{40,37} R. Vainio,⁵⁰ M. Valencia-Otero,⁴⁷ E. Valente,^{41,42} E. Valtonen,⁵⁰ M. Vázquez Acosta,²⁷ M. Vecchi,¹⁸ M. Velasco,³⁰ J. P. Vialle,³ C. X. Wang,²³ L. Wang,⁵ L. Q. Wang,²³ N. H. Wang,²³ Q. L. Wang,⁵ S. Wang,²¹ X. Wang,¹⁰ Yu Wang,²³ Z. M. Wang,²⁴ J. Wei,^{16,24} Z. L. Weng,¹⁰ H. Wu,³⁵ Y. Wu,²⁴ J. N. Xiao,²⁰ R. Q. Xiong,³⁵ X. Z. Xiong,²⁰ W. Xu,^{23,24} Q. Yan,¹⁰ H. T. Yang,^{6,7} Y. Yang,⁴⁴ I. I. Yashin,³⁴ A. Yelland,¹⁰ H. Yi,³⁵ Y. H. You,^{6,7} Y. M. Yu,¹⁰ Z. Q. Yu,⁶ M. Zannoni,^{32,33} C. Zhang,⁶ F. Zhang,⁶ F. Z. Zhang,^{6,7} J. Zhang,²³ J. H. Zhang,³⁵ Z. Zhang,¹⁰ F. Zhao,^{6,7} C. Zheng,²⁴ Z. M. Zheng,⁴ H. L. Zhuang,⁶ V. Zhukov,¹ A. Zichichi,^{8,9} and P. Zucco^{48,49}

(AMS Collaboration)

¹*Physics Institute and JARA-FAME, RWTH Aachen University, 52056 Aachen, Germany*

²*Department of Physics, Middle East Technical University (METU), 06800 Ankara, Türkiye*

³*Université Grenoble Alpes, Université Savoie Mont Blanc, CNRS, LAPP-IN2P3, 74000 Annecy, France*

⁴*Beihang University (BUAA), Beijing 100191, China*

⁵*Institute of Electrical Engineering (IEE), Chinese Academy of Sciences, Beijing 100190, China*

⁶*Institute of High Energy Physics (IHEP), Chinese Academy of Sciences, Beijing 100049, China*

⁷*University of Chinese Academy of Sciences (UCAS), Beijing 100049, China*

⁸*INFN Sezione di Bologna, 40126 Bologna, Italy*

⁹*Università di Bologna, 40126 Bologna, Italy*

¹⁰*Massachusetts Institute of Technology (MIT), Cambridge, Massachusetts 02139, USA*

¹¹*East-West Center for Space Science, University of Maryland, College Park, Maryland 20742, USA*

¹²*IPST, University of Maryland, College Park, Maryland 20742, USA*

¹³*CHEP, Kyungpook National University, 41566 Daegu, Korea*

¹⁴*CNR-IROE, 50125 Firenze, Italy*

¹⁵*European Organization for Nuclear Research (CERN), 1211 Geneva 23, Switzerland*

- ¹⁶DPNC, Université de Genève, 1211 Genève 4, Switzerland
- ¹⁷Université Grenoble Alpes, CNRS, Grenoble INP, LPSC-IN2P3, 38000 Grenoble, France
- ¹⁸Kapteyn Astronomical Institute, University of Groningen, P.O. Box 800, 9700 AV Groningen, Netherlands
- ¹⁹Sun Yat-Sen University (SYSU), Guangzhou 510275, China
- ²⁰Zhejiang University (ZJU), Hangzhou 310058, China
- ²¹Physics and Astronomy Department, University of Hawaii, Honolulu, Hawaii 96822, USA
- ²²National Aeronautics and Space Administration Johnson Space Center (JSC), Houston, Texas 77058, USA
- ²³Shandong University (SDU), Jinan, Shandong 250100, China
- ²⁴Shandong Institute of Advanced Technology (SDIAT), Jinan, Shandong 250100, China
- ²⁵Jülich Supercomputing Centre and JARA-FAME, Research Centre Jülich, 52425 Jülich, Germany
- ²⁶Institut für Experimentelle und Angewandte Physik, Christian-Alberts-Universität zu Kiel, 24118 Kiel, Germany
- ²⁷Instituto de Astrofísica de Canarias (IAC), 38205 La Laguna, and Departamento de Astrofísica, Universidad de La Laguna, 38206 La Laguna, Tenerife, Spain
- ²⁸Laboratório de Instrumentação e Física Experimental de Partículas (LIP), 1649-003 Lisboa, Portugal
- ²⁹National Chung-Shan Institute of Science and Technology (NCSIST), Longtan, Tao Yuan 32546, Taiwan
- ³⁰Centro de Investigaciones Energéticas, Medioambientales y Tecnológicas (CIEMAT), 28040 Madrid, Spain
- ³¹Instituto de Física, Universidad Nacional Autónoma de México (UNAM), Ciudad de México, 01000 Mexico
- ³²INFN Sezione di Milano-Bicocca, 20126 Milano, Italy
- ³³Università di Milano-Bicocca, 20126 Milano, Italy
- ³⁴NRNU MEPhI (Moscow Engineering Physics Institute), Moscow, 115409 Russia
- ³⁵Southeast University (SEU), Nanjing 210096, China
- ³⁶Sodankylä Geophysical Observatory and Space Physics and Astronomy Research Unit, University of Oulu, 90014 Oulu, Finland
- ³⁷INFN Sezione di Perugia, 06100 Perugia, Italy
- ³⁸Università di Perugia, 06100 Perugia, Italy
- ³⁹INFN Sezione di Pisa, 56100 Pisa, Italy
- ⁴⁰Agenzia Spaziale Italiana (ASI), 00133 Roma, Italy
- ⁴¹INFN Sezione di Roma 1, 00185 Roma, Italy
- ⁴²Università di Roma La Sapienza, 00185 Roma, Italy
- ⁴³INFN Sezione di Roma Tor Vergata, 00133 Roma, Italy
- ⁴⁴National Cheng Kung University, Tainan 70101, Taiwan
- ⁴⁵Academia Sinica Grid Center (ASGC), Nankang, Taipei 11529, Taiwan
- ⁴⁶Institute of Physics, Academia Sinica, Nankang, Taipei 11529, Taiwan
- ⁴⁷Physics Department and Center for High Energy and High Field Physics, National Central University (NCU), Tao Yuan 32054, Taiwan
- ⁴⁸INFN TIFPA, 38123 Trento, Italy
- ⁴⁹Università di Trento, 38123 Trento, Italy
- ⁵⁰Space Research Laboratory, Department of Physics and Astronomy, University of Turku, 20014 Turku, Finland



(Received 9 February 2023; revised 28 March 2023; accepted 27 April 2023; published 25 May 2023)

We report the properties of primary cosmic-ray sulfur (S) in the rigidity range 2.15 GV to 3.0 TV based on 0.38×10^6 sulfur nuclei collected by the Alpha Magnetic Spectrometer experiment (AMS). We observed that above 90 GV the rigidity dependence of the S flux is identical to the rigidity dependence of Ne-Mg-Si fluxes, which is different from the rigidity dependence of the He-C-O-Fe fluxes. We found that, similar to N, Na, and Al cosmic rays, over the entire rigidity range, the traditional primary cosmic rays S, Ne, Mg, and C all have sizeable secondary components, and the S, Ne, and Mg fluxes are well described by the weighted sum of the primary silicon flux and the secondary fluorine flux, and the C flux is well described by the weighted sum of the primary oxygen flux and the secondary boron flux. The primary and secondary contributions of the traditional primary cosmic-ray fluxes of C, Ne, Mg, and S (even Z elements) are distinctly different from the primary and secondary contributions of the N, Na, and Al (odd Z elements) fluxes. The abundance ratio at the source for S/Si is 0.167 ± 0.006 , for Ne/Si is 0.833 ± 0.025 , for Mg/Si is 0.994 ± 0.029 , and for C/O is 0.836 ± 0.025 . These values are determined independent of cosmic-ray propagation.

DOI: [10.1103/PhysRevLett.130.211002](https://doi.org/10.1103/PhysRevLett.130.211002)

Sulfur nuclei in cosmic rays are thought to be mainly produced and accelerated in astrophysical sources [1]. Previously, AMS found that the Ne, Mg, and Si primary cosmic-ray fluxes have an identical rigidity dependence above 86.5 GV and that their rigidity dependence is distinctly different from the rigidity dependence of primary cosmic rays He, C, O, and Fe. This shows that Ne-Mg-Si and He-C-O-Fe are two different classes of primary cosmic rays [2,3]. The rigidity dependence of the S flux compared to the Ne-Mg-Si and He-C-O-Fe classes provides new insights into the origin and propagation of cosmic rays [4,5].

Over the last 50 years, a few experiments have measured the S flux in cosmic rays in kinetic energy per nucleon [6–13]. The measurement errors exceed 30% at ~ 50 GeV/n (~ 100 GV in rigidity). There are no previous measurements of the S flux in rigidity.

In this Letter, we report the precise measurement of the S flux in cosmic rays in the rigidity range from 2.15 GV to 3.0 TV based on 0.38×10^6 sulfur nuclei collected by AMS during the first ten years (May 19, 2011 to May 6, 2021) of operation aboard the International Space Station (ISS). The total flux error at 100 GV is 5%.

Detector.—The layout and description of the AMS detector are presented in Refs. [14,15] and shown in Fig. S1 of the Supplemental Material (SM) [16]. The key elements used in this measurement are the permanent magnet [17], the nine layers, $L1$ – $L9$, of the silicon tracker [18–21], and the four planes of the time of flight (TOF) scintillation counters [22]. As an example, Fig. S2 of SM [16] shows the measured tracker coordinate accuracy of $6.2 \mu\text{m}$ in the bending direction together with the Monte Carlo (MC) simulation. Further information on the AMS layout, performance, trigger, and the MC simulations [23–25] is included in SM [16].

Event selection.—In the first ten years, AMS has collected 1.8×10^{11} cosmic-ray events. Sulfur events are required to be downward going and to have a reconstructed track in the inner tracker that passes through $L1$. See Fig. S3 of SM [16] for a reconstructed sulfur event. In the highest rigidity region, $R \geq 1.2$ TV, the track is also required to pass through $L9$. Details of the event selection are contained in the SM [16] and in Refs. [23,26–28].

With this selection, the charge confusion from noninteracted nuclei due to the finite AMS charge resolution is negligible, $< 0.1\%$ over the entire rigidity range; see Fig. S4 of SM [16]. The main sources of background come from interactions of heavier nuclei, such as Cl, Ar, Ca, and Fe, in the AMS materials above tracker $L2$. The background resulting from interactions in the material between $L1$ and $L2$ (transition radiation detector and upper TOF) is evaluated by fitting the charge distribution of tracker $L1$ with charge distribution templates of S, Cl, and Ar, as shown in Fig. S5 of SM [16]. After the cut on the $L1$ charge, the residual background is $< 0.6\%$ over the entire rigidity range. The background from interactions on materials above $L1$ (thin support structures made by carbon fiber and aluminum

honeycomb) has been estimated from simulation using MC samples generated according to AMS flux measurements [3,29] and is $< 3\%$ over the entire rigidity range.

After background subtraction we obtain 0.38×10^6 sulfur nuclei.

Data analysis.—The isotropic flux Φ_i in the i th rigidity bin ($R_i, R_i + \Delta R_i$) is given by

$$\Phi_i = \frac{N_i}{A_i \epsilon_i T_i \Delta R_i}, \quad (1)$$

where N_i is the number of events corrected for bin-to-bin migration, A_i is the effective acceptance including geometric acceptance, event reconstruction and selection efficiencies, and inelastic interactions of nuclei in the AMS materials, ϵ_i is the trigger efficiency, and T_i is the collection time. In this Letter, the flux was measured in 48 bins from 2.15 GV to 3.0 TV, with bin widths chosen according to the rigidity resolution and available statistics.

The bin-to-bin migration of events was corrected using the unfolding procedure described in Ref. [28]. These corrections, $(N_i - \mathfrak{N}_i)/\mathfrak{N}_i$ where \mathfrak{N}_i is the number of observed events in bin i , are $+24\%$ at 3 GV changing smoothly to $+8\%$ at 10 GV, $+1\%$ at 100 GV, -8% at 300 GV, and -5% at 3.0 TV.

Extensive studies were made of the systematic errors. These errors include the uncertainties in the background evaluation discussed above, the trigger efficiency, the geomagnetic cutoff factor [16], the acceptance calculation, the rigidity resolution function, and the absolute rigidity scale.

The systematic error on the flux due to background subtraction is $< 0.5\%$ over the entire rigidity range.

The systematic error on the flux associated with the trigger efficiency measurement is $< 1\%$ over the entire rigidity range.

The geomagnetic cutoff factor was varied from 1.0 to 1.4, resulting in a negligible systematic uncertainty ($< 0.1\%$) in the rigidity range below 30 GV.

The effective acceptances A_i were calculated using MC simulation and corrected for small differences between the data and simulated events related to (a) event reconstruction and selection, namely in the efficiencies of velocity vector determination, track finding, charge determination, and tracker quality cuts and (b) the details of inelastic interactions of nuclei in the AMS materials. The total corrections to the effective acceptance from the differences between data and MC simulation were found to be $< 5\%$ over the entire rigidity range. The systematic error on the flux associated with the reconstruction and selection is $< 3\%$ over the entire rigidity range. The survival probabilities of S nuclei due to interactions in the AMS materials were evaluated using inelastic cross sections measured by AMS as described in Ref. [25]. The uncertainty in the inelastic cross sections is $< 4\%$ up to 100 GV. Above 100 GV, the small rigidity dependence of the cross

section from the Glauber-Gribov model [24] was treated as an uncertainty and added in quadrature to the uncertainties from the measured inelastic cross sections. The overall systematic error on the S flux is $< 4\%$ up to 100 GV and rises smoothly to 6% at 3.0 TV.

The rigidity resolution function has a pronounced Gaussian core characterized by width σ and non-Gaussian tails more than 2.5σ away from the center [23]. The systematic error on the flux due to the rigidity resolution function was obtained by repeating the unfolding procedure while varying the width of the Gaussian core of the resolution function by 5% and by independently varying the amplitudes of the non-Gaussian tails by 10% [23]. The resulting systematic error on the flux is 5% at 2 GV, $< 1\%$ from 3 to 300 GV and increases smoothly to 3% at 3.0 TV.

There are two contributions to the systematic uncertainty on the rigidity scale [28,30]. The first is due to time dependent residual tracker misalignment. This error was estimated by comparing the E/p ratio for electrons and positrons, where E is the energy measured with the electromagnetic calorimeter and p is the momentum measured with the tracker. It was found to be $1/34 \text{ TV}^{-1}$ [21]. The second systematic error on the rigidity scale arises from the magnetic field map measurement and its temperature corrections [28]. The overall error on the flux due to uncertainty on the rigidity scale is $< 1\%$ up to 300 GV and increases smoothly to 5.5% at 3 TV.

Most importantly, several independent analyses were performed on the same data sample by different study groups. The results of those analyses are consistent with this Letter.

Results.—The measured sulfur flux Φ_S including statistical and systematic errors is reported in Table SI of SM [16] as a function of the rigidity at the top of the AMS detector. To compare the rigidity dependence of the sulfur flux with the primary cosmic-ray O, Ne, Mg, and Si fluxes, and the secondary cosmic-ray F flux, the measurements of the O, Ne, Mg, and Si [14], and F [31] fluxes were extended to the ten-year period and rebinned in the same Φ_S rigidity bins. They are reported in Tables SII to SVI of SM [16]. Figure 1(a) shows the AMS Φ_S as a function of rigidity with the total errors, together with the Ne, Mg, and Si fluxes. As seen, the rigidity dependences of the S, Ne, and Mg fluxes are very similar, but are different from the Si flux at low rigidities. The rigidity dependences of all four fluxes are identical at high rigidities. Figure 1(b) shows the ten-year AMS C and O fluxes—see also Tables SVII and SVIII of SM [16]—as a function of rigidity. As seen, the rigidity dependences of the C and O fluxes are identical at high rigidities, but also different at low rigidities. These observed differences indicate that at low rigidities sizeable fractions of the C, Ne, Mg, and S fluxes have a secondary origin [32].

In Fig. 1 and subsequent figures the data points are placed along the abscissa at \tilde{R} calculated for a flux $\propto R^{-2.7}$ [33].

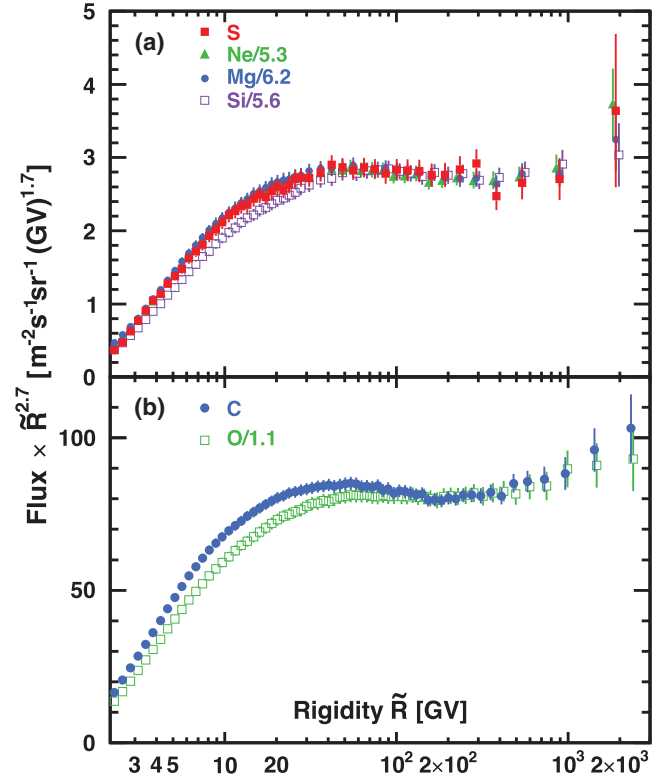


FIG. 1. (a) The AMS S flux multiplied by $\tilde{R}^{2.7}$ with total errors as a function of rigidity together with the AMS Ne, Mg, and Si fluxes. As seen, rigidity dependences of S, Ne, and Mg fluxes are very similar, and are different from Si flux at low rigidities. The rigidity dependences of all four fluxes are identical at high rigidities. (b) The AMS C and O fluxes multiplied by $\tilde{R}^{2.7}$ with total errors as functions of rigidity. As seen, rigidity dependences of C and O fluxes are identical at high rigidities, but also different at low rigidities. For clarity, the Ne, Si, and O data points above 50 GV are displaced horizontally, and, for display purposes only, Ne, Mg, Si, and O fluxes were rescaled as indicated.

Figure 2 shows the AMS Φ_S as a function of kinetic energy per nucleon E_K together with other measurements [6–12]. Data from other experiments have been extracted using Ref. [34]. Also shown in the figure is the prediction of the latest GALPROP-HELMOD cosmic-ray propagation model [5].

To further examine the rigidity dependence of Φ_S , the variation of the flux spectral index with rigidity was obtained in a model-independent way from $\gamma = d[\log(\Phi)]/d[\log(R)]$ over nonoverlapping rigidity intervals bounded by 5.9, 11.0, 16.6, 28.8, 45.1, 80.5, 211.0, and 3000.0 GV. The results are presented in Fig. S6 of SM [16] in comparison with the spectral indices of the Ne, Mg, and Si fluxes. As seen, in the rigidity range 5.9 to 80.5 GV, the Ne, Mg, and S spectral indices are all lower than Si spectral index, and the spectral indices of four elements are identical above ~ 80 GV.

To establish the rigidity intervals where the S, Ne, Mg, and Si fluxes have identical rigidity dependence, the S/Ne,

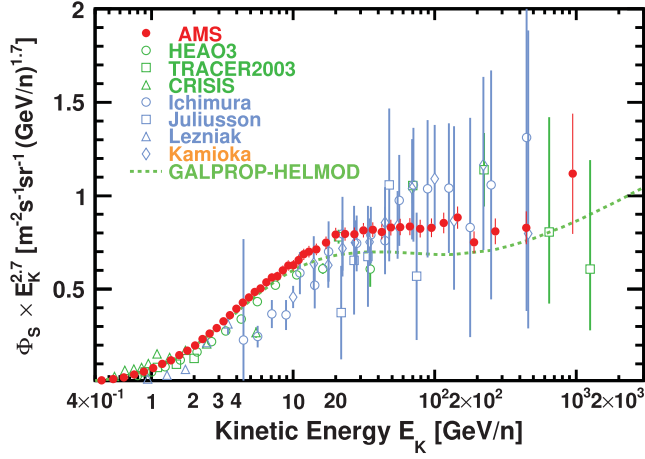


FIG. 2. The AMS sulfur flux Φ_S as a function of kinetic energy per nucleon E_K multiplied by $E_K^{2.7}$ together with other measurements [6–12]. For the AMS measurements $E_K = (\sqrt{Z^2 \tilde{R}^2 + M^2} - M)/A$ where Z , M , and A are the $^{32}_{16}\text{S}$ nuclear charge, mass, and atomic mass number, respectively. The dashed green curve shows prediction of the latest GALPROP-HELMOD [5] model.

S/Mg, and S/Si flux ratios were computed using the data in Tables SI, SIII, SIV, and SV of SM [16] and fitted above 5.9 GV with

$$\frac{\Phi_S}{\Phi_{\text{Ne,Mg,Si}}} = \begin{cases} k(R/R_0)^\Delta, & R \leq R_0, \\ k, & R > R_0. \end{cases} \quad (2)$$

The results are shown in Figs. 3(a)–3(c). For Φ_S/Φ_{Ne} , the fit yields $k^{S/\text{Ne}} = 0.194 \pm 0.004$, $R_0^{S/\text{Ne}} = 77 \pm 37$ GV, and $\Delta^{S/\text{Ne}} = 0.022 \pm 0.008$ with a $\chi^2/\text{d.o.f.} = 22/35$; see Fig. 3(a). For Φ_S/Φ_{Mg} , the fit yields $k^{S/\text{Mg}} = 0.161 \pm 0.004$, $R_0^{S/\text{Mg}} = 99 \pm 47$ GV, and $\Delta^{S/\text{Mg}} = 0.015 \pm 0.006$ with a $\chi^2/\text{d.o.f.} = 20/35$; see Fig. 3(b). For Φ_S/Φ_{Si} , the fit yields $k^{S/\text{Si}} = 0.181 \pm 0.005$, $R_0^{S/\text{Si}} = 87 \pm 18$ GV, and $\Delta^{S/\text{Si}} = -0.046 \pm 0.006$ with a $\chi^2/\text{d.o.f.} = 20/35$; see Fig. 3(c). The significance of the break around 90 GV was estimated by comparing χ^2 values for fits with Eq. (2) and fits with Eq. (2) with R_0 fixed to 3 TV. It was found to be 2.35σ for Φ_S/Φ_{Ne} , 1.30σ for Φ_S/Φ_{Mg} , and 2.95σ for Φ_S/Φ_{Si} . This shows that all four fluxes have an identical rigidity dependence above $R_0 \sim 90$ GV and that S belongs to the Ne-Mg-Si primary cosmic-ray class.

Previously, AMS found that the rigidity dependence of the Ne, Mg, and Si spectra is distinctly different from the rigidity dependence of primary cosmic rays He-C-O, so that above 86.5 GV the Ne/O, Mg/O, and Si/O flux ratios can be described by a simple power law $\propto R^\delta$ with average $\langle \delta \rangle = -0.045 \pm 0.008$ [2]. To directly compare the Φ_S and Φ_O rigidity dependence the S/O flux ratio was computed using the data in Tables SI and SII of SM [16] and was fitted with

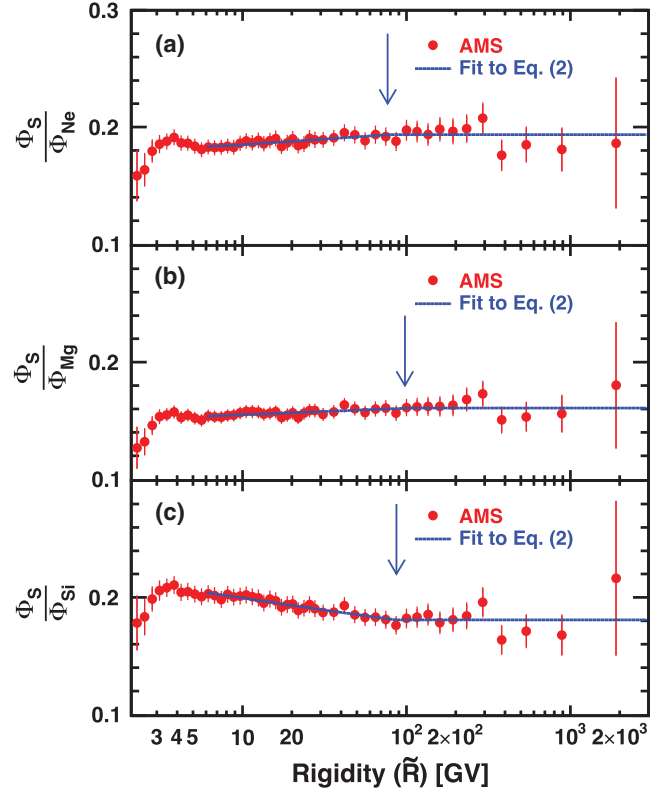


FIG. 3. The AMS (a) Φ_S/Φ_{Ne} , (b) Φ_S/Φ_{Mg} , and (c) Φ_S/Φ_{Si} with their total errors as functions of rigidity. The solid curves show the fit results with Eq. (2). As seen, the four fluxes (Ne, Mg, Si, and S) have identical rigidity dependence above $R_0 \sim 90$ GV, as indicated by the location of the arrows.

$$\frac{\Phi_S}{\Phi_O} = \begin{cases} C(R/86.5 \text{ GV})^\Delta, & R \leq 86.5 \text{ GV}, \\ C(R/86.5 \text{ GV})^\delta, & R > 86.5 \text{ GV}, \end{cases} \quad (3)$$

similar to Eq. (4) of Ref. [2] above 20 GV. The fit yields $\delta = -0.05 \pm 0.02$ in excellent agreement with the average $\langle \delta \rangle = -0.045 \pm 0.008$ of Ne/O, Mg/O, and Si/O. This verifies that S, like Ne-Mg-Si does not belong to He-C-O-Fe class of primary cosmic rays. Figure S7 of SM [16] shows the Φ_S/Φ_O together with the fit results. Similarly, fitting above 5.9 GV the S/Ne, S/Mg, and S/Si flux ratios with Eq. (3), we obtained $\delta^{S/\text{Ne}} = -0.008 \pm 0.019$, $\delta^{S/\text{Mg}} = 0.006 \pm 0.019$, and $\delta^{S/\text{Si}} = -0.011 \pm 0.020$, all compatible with zero, which confirms that S, Ne, Si, and Mg fluxes have an identical rigidity dependence above ~ 90 GV; see Fig. S8 of SM [16] for fit results.

To understand the difference in the rigidity dependence at low rigidities of the Si and the Ne, Mg, and S fluxes, and of the O and C flux, we used the method described in Refs. [35,36]. To obtain the primary Φ^P and secondary Φ^S components of the Ne, Mg, and S fluxes, we fit $\Phi_{\text{Ne}} = \Phi_{\text{Ne}}^P + \Phi_{\text{Ne}}^S$, $\Phi_{\text{Mg}} = \Phi_{\text{Mg}}^P + \Phi_{\text{Mg}}^S$, and $\Phi_S = \Phi_S^P + \Phi_S^S$ to the weighted sums of a characteristic heavy primary cosmic-ray flux, namely silicon Φ_{Si} , and of a characteristic

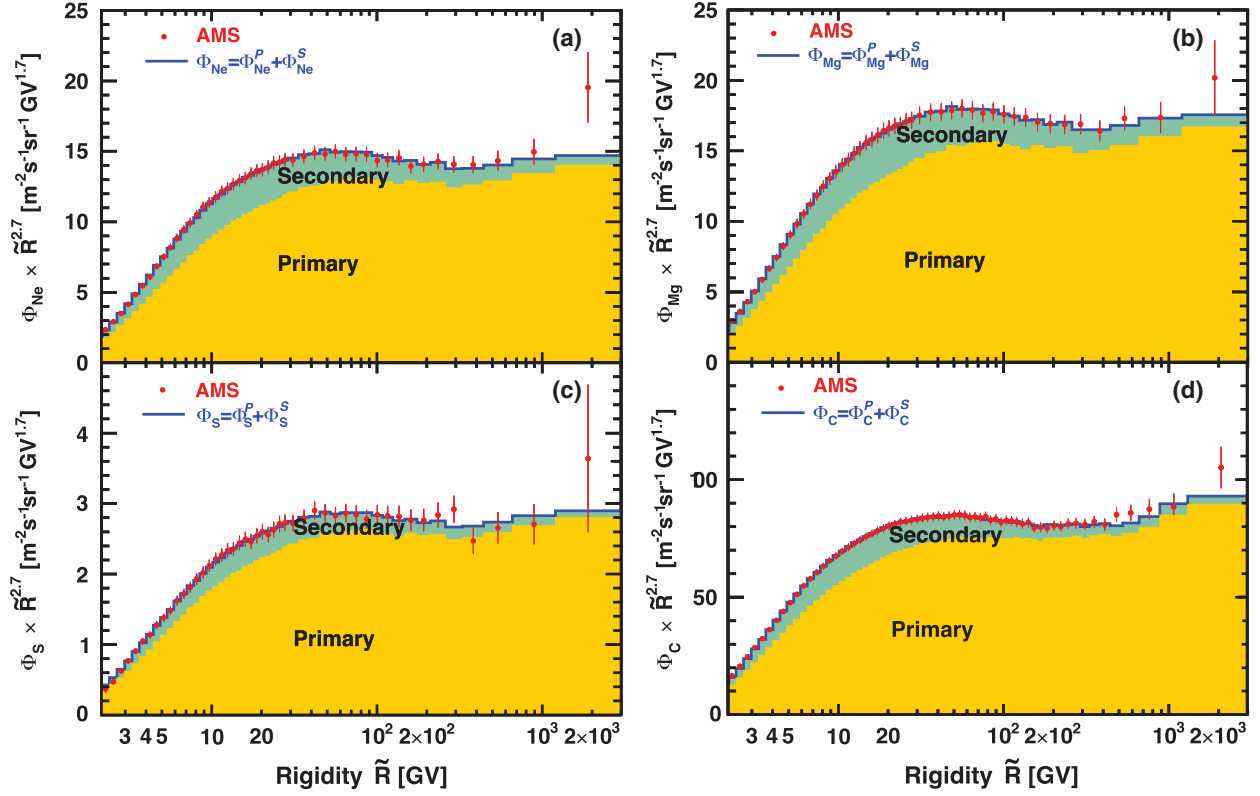


FIG. 4. The AMS (a) Φ_{Ne} , (b) Φ_{Mg} , (c) Φ_{S} with total errors together with fits to the weighted sum of the Si flux Φ_{Si} and the F flux Φ_{F} , and (d) AMS Φ_{C} with total errors together with fit to the weighted sum of the O flux Φ_{O} and the B flux Φ_{B} . In (a), (b), (c), and (d) the fit results are shown by blue curves and the contributions of the primary and secondary components are indicated by the yellow and green shadings, respectively. The fits are in excellent agreement with the data over entire rigidity range.

heavy secondary cosmic ray flux, namely fluorine Φ_{F} , over the entire rigidity range. The fits yield $\Phi_{\text{Ne}}^{\text{P}} = (0.833 \pm 0.025) \times \Phi_{\text{Si}}$ and $\Phi_{\text{Ne}}^{\text{S}} = (2.07 \pm 0.14) \times \Phi_{\text{F}}$ with a $\chi^2/\text{d.o.f.} = 26/47$, $\Phi_{\text{Mg}}^{\text{P}} = (0.994 \pm 0.029) \times \Phi_{\text{Si}}$ and $\Phi_{\text{Mg}}^{\text{S}} = (2.59 \pm 0.19) \times \Phi_{\text{F}}$ with a $\chi^2/\text{d.o.f.} = 22/47$, and $\Phi_{\text{S}}^{\text{P}} = (0.167 \pm 0.006) \times \Phi_{\text{Si}}$ and $\Phi_{\text{S}}^{\text{S}} = (0.28 \pm 0.05) \times \Phi_{\text{F}}$ with a $\chi^2/\text{d.o.f.} = 23/47$, as shown in Figs. 4(a)–4(c), respectively. Similarly, we have analyzed the C flux from

Table SVII of SM [16], $\Phi_{\text{C}} = \Phi_{\text{C}}^{\text{P}} + \Phi_{\text{C}}^{\text{S}}$ by fitting it to the weighted sum of the primary oxygen flux Φ_{O} from Table SVIII of SM [16], and the corresponding ten-year secondary boron flux Φ_{B} from Table SIX of SM [16]. The fit yields $\Phi_{\text{C}}^{\text{P}} = (0.836 \pm 0.025) \times \Phi_{\text{O}}$ and $\Phi_{\text{C}}^{\text{S}} = (0.67 \pm 0.02) \times \Phi_{\text{B}}$ with a $\chi^2/\text{d.o.f.} = 30/65$ as shown in Fig. 4(d).

Figure S9 of SM [16] details the Ne, Mg, S, and C primary and secondary components rigidity dependence. As seen

TABLE I. The primary and secondary components of C ($Z = 6$), Ne ($Z = 8$), Mg ($Z = 10$), and S ($Z = 16$), as well as of N ($Z = 7$), Na ($Z = 11$), and Al ($Z = 13$) [36] fluxes and their primary fractions at 6 GV, 100 GV, and 2 TV. As seen, the primary and secondary contributions of the even Z element fluxes of C, Ne, Mg, and S are distinctly different from the primary and secondary contributions of the odd Z element N, Na, and Al fluxes.

| Nuclei flux | Primary | Secondary | Primary fraction, % | | |
|--------------------|---|--|---------------------|--------------|--------------|
| | | | 6 GV | 100 GV | 2 TV |
| Φ_{C} | $(0.836 \pm 0.025) \times \Phi_{\text{O}}$ | $(0.67 \pm 0.02) \times \Phi_{\text{B}}$ | 80 ± 1 | 91 ± 0.5 | 96 ± 0.5 |
| Φ_{Ne} | $(0.833 \pm 0.025) \times \Phi_{\text{Si}}$ | $(2.07 \pm 0.14) \times \Phi_{\text{F}}$ | 76 ± 1 | 89 ± 1 | 95 ± 0.5 |
| Φ_{Mg} | $(0.994 \pm 0.029) \times \Phi_{\text{Si}}$ | $(2.59 \pm 0.19) \times \Phi_{\text{F}}$ | 75 ± 1 | 89 ± 1 | 95 ± 0.5 |
| Φ_{S} | $(0.167 \pm 0.006) \times \Phi_{\text{Si}}$ | $(0.28 \pm 0.05) \times \Phi_{\text{F}}$ | 82 ± 3 | 91 ± 1 | 97 ± 1 |
| Φ_{N} | $(0.092 \pm 0.002) \times \Phi_{\text{O}}$ | $(0.61 \pm 0.02) \times \Phi_{\text{B}}$ | 31 ± 1 | 56 ± 1 | 77 ± 3 |
| Φ_{Na} | $(0.036 \pm 0.003) \times \Phi_{\text{Si}}$ | $(1.36 \pm 0.04) \times \Phi_{\text{F}}$ | 17 ± 2 | 35 ± 2 | 62 ± 12 |
| Φ_{Al} | $(0.103 \pm 0.004) \times \Phi_{\text{Si}}$ | $(1.04 \pm 0.03) \times \Phi_{\text{F}}$ | 43 ± 1 | 67 ± 1 | 78 ± 8 |

from the figure, above ~ 4 GV the contributions of the secondary component in all fluxes decrease with rigidity, and the contributions of the primary component increase. Note, that contributions of the primary component are above 70% for all four fluxes over the entire rigidity range.

Table I summarizes the primary and secondary components of the C, Ne, Mg, and S fluxes together with the primary fractions at different rigidities, as well as that of N, Na, and Al from Ref. [36]. As seen, the primary and secondary contributions of the traditional primary cosmic-ray fluxes of C, Ne, Mg, and S (even Z elements) are distinctly different from the primary and secondary contributions of the N, Na, and Al (odd Z elements) fluxes.

The observation that the traditional primary cosmic-ray C, Ne, Mg, and S fluxes are the linear combinations of primary and secondary fluxes permits the direct determination of the C/O, Ne/Si, Mg/Si, and S/Si abundance ratios at the source without the need to consider the Galactic propagation of cosmic rays, see the SM of Ref. [36]. Table SX of SM [16] shows AMS model-independent results on the cosmic nuclei flux ratios at the source over a wide energy range together with earlier model-dependent results from low-energy measurements [6,37–39].

In conclusion, we have presented precision measurement of the sulfur flux rigidity dependence from 2.15 GV to 3.0 TV with detailed studies of the systematic errors. We observed that above 90 GV the rigidity dependence of the sulfur flux is identical to the rigidity dependence of the Ne-Mg-Si fluxes, which is different from the rigidity dependence of the He-C-O-Fe fluxes. This shows that S belongs to the Ne-Mg-Si class of primary cosmic rays. The result is new and unexpected. Most interesting, we found that, similar to N, Na, and Al cosmic rays, over the entire rigidity range, the traditional primary cosmic rays S, Ne, Mg, and C all have sizeable secondary components, and the S, Ne, and Mg fluxes are well described by the weighted sum of the primary silicon flux and the secondary fluorine flux, and the C flux is well described by the weighted sum of the primary oxygen flux and the secondary boron flux. The primary and secondary contributions of the traditional primary cosmic-ray fluxes of C, Ne, Mg, and S (even Z elements) are distinctly different from the primary and secondary contributions of the N, Na, and Al (odd Z elements) fluxes. The abundance ratio at the source for S/Si is 0.167 ± 0.006 , for Ne/Si is 0.833 ± 0.025 , for Mg/Si is 0.994 ± 0.029 , and for C/O is 0.836 ± 0.025 . These values are determined independent of cosmic-ray propagation.

We are grateful for important physics discussions with Igor Moskalenko and Subir Sarkar. We thank former NASA Administrator Daniel S. Goldin for his dedication to the legacy of the ISS as a scientific laboratory and his decision for NASA to fly AMS as a DOE payload. We also acknowledge the continuous support of the NASA leadership, particularly Kathryn Lueders and of the JSC and

MSFC flight control teams that have allowed AMS to operate optimally on the ISS for over eleven years. We are grateful for the support of Glen Crawford of the DOE including resources from the National Energy Research Scientific Computing Center under Contract No. DE-AC02-05CH11231. We gratefully acknowledge the strong support from CERN including Fabiola Gianotti, and the CERN IT department including Bernd Panzer-Steindel. We also acknowledge the continuous support from MIT and its School of Science, Nergis Mavalvala, and the Laboratory for Nuclear Science, Boleslaw Wyslouch. Research supported by Chinese Academy of Sciences, Institute of High Energy Physics, Institute of Electrical Engineering, China Academy of Space Technology, National Natural Science Foundation (NSFC), and Ministry of Science and Technology, National Key R&D Program Grants No. 2022YFA1604802 and No. 2022YFA1604803, NSFC Grant No. 12275158, the China Scholarship Council, the provincial governments of Shandong, Jiangsu, Guangdong, Shandong University, and the Shandong Institute of Advanced Technology, China; the Academy of Finland, Project No. 321882, Finland; CNRS/IN2P3 and CNES, France; DLR under Grants No. 500O1803 and computing support on the JARA Partition of the RWTH Aachen supercomputer, Germany; INFN and ASI under ASI-INFN Agreements No. 2019-19-HH.0, its amendments, and No. 2021-43-HH.0 and ASI-University of Perugia Agreement No. 2019-2-HH.0, Italy; CHEP and NRF under Grant No. NRF-2018R1A6A1A06024970 at Kyungpook National University, Korea; the Consejo Nacional de Ciencia y Tecnología and UNAM, Mexico; NWO under Grant No. 680-1-004, Netherlands; FCT under Grant No. CERN/FIS-PAR/0013/2019, Portugal; the Ministry of Science and Higher Education under Project No. 0723-2020-0040, Russia; CIEMAT, IAC, CDTI, and SEIDI-MINECO under Grants No. PID2019-107988 GB-C21/C22, and No. CEX2019-000920-S, Spain; the Fondation Dr. Manfred Steuer, Switzerland; Academia Sinica, the National Science and Technology Council (NSTC), formerly the Ministry of Science and Technology (MOST), under Grants No. 111-2123-M-001-004 and No. 111-2112-M-006-029, High Education Sprout Project by the Ministry of Education at National Cheng Kung University, former Presidents of Academia Sinica Yuan-Tseh Lee and Chi-Huey Wong and former Ministers of NSTC (formerly MOST) Maw-Kuen Wu and Luo-Chuan Lee, Taiwan; the Turkish Energy, Nuclear and Mineral Research Agency (TENMAK) under Grant No. 2020TAEK(CERN) A5.H1.F5-26, Turkey; and NSF Grant No. 2013228 and ANSWERS proposals No. 2149809, No. 2149810, and No. 2149811, LWS NASA Grant/Cooperative Agreement No. 80NSSC20K1819, and NASA Grant No. 80NSSC21K1392, USA.

- *Also at Nikhef, 1098 XG Amsterdam, Netherlands.
 †Also at IRCCS Azienda Ospedaliero-Universitaria di Bologna, Bologna, Italy.
- [1] I. A. Grenier, J. H. Black, and A. W. Strong, The nine lives of cosmic rays in galaxies, *Annu. Rev. Astron. Astrophys.* **53**, 199 (2015); P. Blasi, The origin of galactic cosmic rays, *Astron. Astrophys. Rev.* **21**, 70 (2013); A. W. Strong, I. V. Moskalenko, and V. S. Ptuskin, Cosmic-ray propagation and interactions in the galaxy, *Annu. Rev. Nucl. Part. Sci.* **57**, 285 (2007); A. Castellina and F. Donato, Diffusion coefficient and acceleration spectrum from direct measurements of charged cosmic ray nuclei, *Astropart. Phys.* **24**, 146 (2005).
- [2] M. Aguilar *et al.*, Properties of Neon, Magnesium, and Silicon Primary Cosmic Rays Results from the Alpha Magnetic Spectrometer, *Phys. Rev. Lett.* **124**, 211102 (2020).
- [3] M. Aguilar *et al.*, Properties of Iron Primary Cosmic Rays: Results from the Alpha Magnetic Spectrometer, *Phys. Rev. Lett.* **126**, 041104 (2021).
- [4] G. Jóhannesson *et al.*, Bayesian analysis of cosmic ray propagation: Evidence against homogeneous diffusion, *Astrophys. J.* **824**, 16 (2016).
- [5] M. J. Boschini *et al.*, Inference of the local interstellar spectra of cosmic-ray nuclei $Z \leq 28$ with GalProp-HelMod framework, *Astrophys. J. Suppl. Ser.* **250**, 27 (2020); M. J. Boschini *et al.*, The discovery of a low-energy excess in cosmic-ray iron: Evidence of the past supernova activity in the local bubble, *Astrophys. J. Suppl. Ser.* **213**, 5 (2021).
- [6] J. J. Engelmann *et al.*, Charge composition and energy spectra of cosmic-ray nuclei for elements from Be to Ni—Results from HEAO-3-C2, *Astron. Astrophys.* **233**, 96 (1990).
- [7] M. Ave, P. J. Boyle, F. Gahbauer, C. Höppner, J. R. Hörandel, M. Ichimura, D. Müller, and A. Romero-Wolf, Composition of primary cosmic-ray nuclei at high energies, *Astrophys. J.* **678**, 262 (2008).
- [8] J. S. Young, P. S. Freier, C. J. Waddington, N. R. Brewster, and R. K. Fickle, The elemental and isotopic composition of cosmic rays—Silicon to nickel, *Astrophys. J.* **246**, 1014 (1981).
- [9] M. Ichimura *et al.*, Observation of heavy cosmic-ray primaries over the wide energy range from 100 GeV/particle to 100 TeV/particle: Is the celebrated ‘knee’ actually so prominent?, *Phys. Rev. D* **48**, 1949 (1993).
- [10] E. Juliusson, Charge composition and energy spectra of cosmic-ray nuclei at energies above 20 GeV per nucleon, *Astrophys. J.* **191**, 331 (1974).
- [11] J. Lezniak and W. Webber, The charge composition and energy spectra of cosmic-ray nuclei from 3000 MeV per nucleon to 50 GeV per nucleon, *Astrophys. J.* **223**, 676 (1978).
- [12] E. Kamioka *et al.*, Azimuthally controlled observation of heavy cosmic-ray primaries by means of the balloon-borne emulsion chamber, *Astropart. Phys.* **6**, 155 (1997).
- [13] K. Lave *et al.*, Galactic cosmic-ray energy spectra and composition during the 2009–2010 solar minimum period, *Astrophys. J.* **770**, 117 (2013).
- [14] M. Aguilar *et al.*, The Alpha Magnetic Spectrometer (AMS) on the international space station: Part II—results from the first seven years, *Phys. Rep.* **894**, 1 (2021).
- [15] A. Kounine, The Alpha Magnetic Spectrometer on the international space station, *Int. J. Mod. Phys. E* **21**, 1230005 (2012); S. Ting, The Alpha Magnetic Spectrometer on the international space station, *Nucl. Phys. B, Proc. Suppl.* **243–244**, 12 (2013); B. Bertucci, The AMS-02 detector operation in space, *Proc. Sci. EPS-HEP2011* (2011) 67; M. Incagli, Astroparticle physics with AMS02, *AIP Conf. Proc.* **1223**, 43 (2010); R. Battiston, The antimatter spectrometer (AMS-02): A particle physics detector in space, *Nucl. Instrum. Methods Phys. Res., Sect. A* **588**, 227 (2008).
- [16] See Supplemental Material at <http://link.aps.org/supplemental/10.1103/PhysRevLett.130.211002> for the details of the detector description and event selection; tabulated S, O, Ne, Mg, Si, F, C, and B fluxes as functions of rigidity; and figures regarding detector layout, tracker coordinate resolution, charge selection, S/O, S/Ne, S/Mg, and S/Si flux ratios, and Ne, Mg, S, and C flux primary and secondary contributions as functions of rigidity.
- [17] K. Lübelmeyer *et al.*, Upgrade of the Alpha Magnetic Spectrometer (AMS-02) for long term operation on the international space station (ISS), *Nucl. Instrum. Methods Phys. Res., Sect. A* **654**, 639 (2011).
- [18] B. Alpat *et al.*, The internal alignment and position resolution of the AMS-02 silicon tracker determined with cosmic-ray muons, *Nucl. Instrum. Methods Phys. Res., Sect. A* **613**, 207 (2010).
- [19] Y. Jia, Q. Yan, V. Choutko, H. Liu, and A. Oliva, Nuclei charge measurement by the Alpha Magnetic Spectrometer silicon tracker, *Nucl. Instrum. Methods Phys. Res., Sect. A* **972**, 164169 (2020).
- [20] G. Ambrosi, V. Choutko, C. Delgado, A. Oliva, Q. Yan, and Y. Li, The spatial resolution of the silicon tracker of the Alpha Magnetic Spectrometer, *Nucl. Instrum. Methods Phys. Res., Sect. A* **869**, 29 (2017).
- [21] Q. Yan and V. Choutko, Alignment of the Alpha Magnetic Spectrometer (AMS) in space, *Eur. Phys. J. C* **83**, 245 (2023).
- [22] V. Bindi *et al.*, Calibration and performance of the AMS-02 time of flight detector in space, *Nucl. Instrum. Methods Phys. Res., Sect. A* **743**, 22 (2014).
- [23] M. Aguilar *et al.*, Precision Measurement of the Helium Flux in Primary Cosmic Rays of Rigidities 1.9 GV to 3 TV with the Alpha Magnetic Spectrometer on the International Space Station, *Phys. Rev. Lett.* **115**, 211101 (2015).
- [24] J. Allison *et al.*, Recent developments in GEANT4, *Nucl. Instrum. Methods Phys. Res., Sect. A* **835**, 186 (2016); GEANT4 developments and applications, *IEEE Trans. Nucl. Sci.* **53**, 270 (2006); S. Agostinelli *et al.*, GEANT4—a simulation toolkit, *Nucl. Instrum. Methods Phys. Res., Sect. A* **506**, 250 (2003).
- [25] Q. Yan, V. Choutko, A. Oliva, and M. Paniccia, Measurements of nuclear interaction cross sections with the Alpha Magnetic Spectrometer on the international space station, *Nucl. Phys.* **A996**, 121712 (2020).
- [26] J. Alcaraz *et al.*, Leptons in near earth orbit, *Phys. Lett. B* **484**, 10 (2000).
- [27] C. C. Finlay *et al.*, International geomagnetic reference field: The eleventh generation, *Geophys. J. Int.* **183**, 1216 (2010); E. Thébaud *et al.*, *Earth Planets Space* **67**, 79 (2015); Geomagnetic Field Modeling Working Group,

- IGRF-13 model, 2019, <https://www.ngdc.noaa.gov/IAGA/vmod/igrf.html>.
- [28] M. Aguilar *et al.*, Precision Measurement of the Proton Flux in Primary Cosmic Rays from Rigidity 1 GV to 1.8 TV with the Alpha Magnetic Spectrometer on the International Space Station, *Phys. Rev. Lett.* **114**, 171103 (2015).
- [29] M. Aguilar *et al.* (AMS Collaboration), Measurement of the heavy nuclei cosmic rays fluxes with the Alpha Magnetic Spectrometer (to be published).
- [30] J. Berdugo, V. Choutko, C. Delgado, and Q. Yan, Determination of the rigidity scale of the Alpha Magnetic Spectrometer, *Nucl. Instrum. Methods Phys. Res., Sect. A* **869**, 10 (2017).
- [31] M. Aguilar *et al.*, Properties of Heavy Secondary Fluorine Cosmic Rays: Results from the Alpha Magnetic Spectrometer, *Phys. Rev. Lett.* **126**, 081102 (2021).
- [32] C. Evoli, R. Aloisio, and P. Blasi, Galactic cosmic rays after the AMS-02 observations, *Phys. Rev. D* **99**, 103023 (2019).
- [33] G. D. Lafferty and T. R. Wyatt, Where to stick your data points: The treatment of measurements within wide bins, *Nucl. Instrum. Methods Phys. Res., Sect. A* **355**, 541 (1995). We have used Eq. (6) with $\tilde{R} \equiv x_{lv}$.
- [34] D. Maurin, F. Melot, and R. Taillet, A database of charged cosmic rays, *Astron. Astrophys.* **569**, A32 (2014).
- [35] M. Aguilar *et al.*, Precision Measurement of Cosmic-Ray Nitrogen and its Primary and Secondary Components with the Alpha Magnetic Spectrometer on the International Space Station, *Phys. Rev. Lett.* **121**, 051103 (2018).
- [36] M. Aguilar *et al.*, Properties of a New Group of Cosmic Nuclei: Results from the Alpha Magnetic Spectrometer on Sodium, Aluminum, and Nitrogen, *Phys. Rev. Lett.* **127**, 021101 (2021).
- [37] M. A. DuVernois and M. R. Thayer, The elemental composition of the galactic cosmic-ray source: Ulysses high-energy telescope results, *Astrophys. J.* **465**, 982 (1996).
- [38] A. C. Cummings, E. C. Stone, B. C. Heikkila, N. Lal, W. R. Webber, G. Jóhannesson, I. V. Moskalenko, E. Orlando, and T. A. Porter, Galactic cosmic rays in the local interstellar medium: Voyager 1 observations and model results, *Astrophys. J.* **831**, 18 (2016).
- [39] M. H. Israel *et al.*, Elemental composition at the cosmic-ray source derived from the ACE-CRIS instrument. I. ${}^6\text{C}$ to ${}^{28}\text{Ni}$, *Astrophys. J.* **865**, 69 (2018).